JACS
JOURNAL OF THE AMERICAN CHEMICAL SOCIETY
Article
Cite This: J. Am. Chem. Soc. XXXX, XXX, XXX-XXX
pubs.acs.org/JACS

Mitochondrial Imaging with Combined Fluorescence and Stimulated Raman Scattering Microscopy Using a Probe of the Aggregation-Induced Emission Characteristic

Xuesong Li,[†,‡,∥] Meijuan Jiang,[§,∥] Jacky W. Y. Lam,[§] Ben Zhong Tang,[*,§] and Jianan Y. Qu[*,†,‡]

[†]Department of Electronic and Computer Engineering, [‡]Center of Systems Biology and Human Health, School of Science, and Institute for Advanced Study, and [§]Department of Chemistry, Hong Kong Branch of the Chinese National Engineering Research Center for Tissue Restoration and Reconstruction, and Division of Biomedical Engineering, Hong Kong University of Science and Technology, Clear Water Bay, Kowloon, Hong Kong China

Supporting Information

ABSTRACT: *In vivo* quantitative measurement of biodistribution plays a critical role in the drug/probe development and diagnosis/treatment process monitoring. In this work, we report a probe, named AIE-SRS-Mito, for imaging mitochondria in live cells via fluorescence (FL) and stimulated Raman scattering (SRS) imaging. The probe features an aggregation-induced emission (AIE) characteristic and possesses an enhanced alkyne Raman peak at 2223 cm^{-1}. The dual-mode imaging of AIE-SRS-Mito for selective mitochondrion-targeting was examined on a homemade FL−SRS microscope system. The detection limit of the probe in the SRS imaging was estimated to be 8.5 μM. Due to the linear concentration dependence of SRS and inertness of the alkyne Raman signal to environmental changes, the intracellular distribution of the probe was studied, showing a local concentration of >2.0 mM in the mitochondria matrix, which was >100-fold higher than the incubation concentration. To the best of our knowledge, this is the first time that the local concentration of AIE molecules inside cells has been measured noninvasively and directly. Also, the nonquenching effect of such AIE molecules in cell imaging has been verified by the positive correlation of FL and SRS signals. Our work will encourage the utilization of SRS microscopy for quantitative characterization of FL probes or other nonfluorescent compounds in living biological systems and the development of FL−SRS dual-mode probes for specific biotargets.

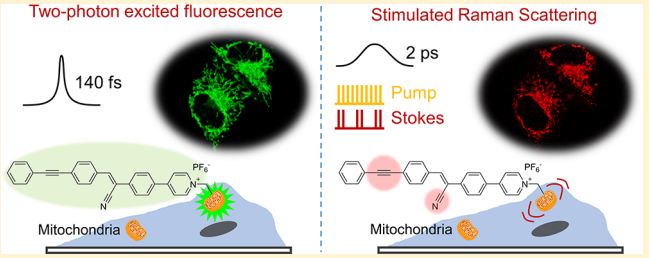

INTRODUCTION

To elucidate the biological functions of fluorescent probes or drugs, it is important to obtain a detailed picture of their intracellular distribution (local concentration) and how they evolve with time. Various imaging methods have been developed, including fluorescence imaging, Raman scattering imaging, magnetic resonance imaging, photoacoustic imaging, ultrasound imaging, X-ray radiography, and positron emission tomography. Among them, fluorescence methods are widely used due to their advantages of simplicity, noninvasiveness, high sensitivity, and high spatiotemporal resolution.[1−5] However, the linear quantification range for fluorescence falls at low solution concentration due to aggregation-caused quenching (ACQ). This problem cannot be satisfyingly relieved by reducing the dye incubation concentration due to the heterogeneity of cells. The dye concentration accumulated in organelles could be much higher than in medium and cytoplasm. For instance, the concentration of cationic lipophilic molecules in the mitochondrion matrix was estimated to be up to 1000-fold higher than that in the cytoplasm, on the basis of the electrophoresis effect driven by the large mitochondrial membrane potential (~180 mV).[6] Such a high concentration would lead to fluorescence quenching, reduced image contrast, and a distortion of the linear relationship of the fluorescence intensity and dye concentration, as exemplified by Rhodamine 123.[7] Besides the concentration effect, many fluorescent probes are found to be highly sensitive to the microenvironment (viscosity and polarity), making the use of fluorescence intensity for interpreting the intracellular local concentration unreliable.[8] Thus, it is of great significance to develop a new method for accurate measurement of intracellular dye distribution, especially at high concentration in living biological systems.

Recently, a series of fluorescent probes with aggregation-induced emission (AIE) characteristics have been reported. Circumventing the fluorescence quenching effect in the aggregated state of traditional fluorescent dyes, such as fluorescein and Rhodamine 123, these AIE probes are weakly emissive in solution and exhibit a "turn-on" feature when binding to targets, showing an ultrahigh imaging contrast, good photostability, and biocompatibility.[9] Although we have observed the increase in fluorescence intensity with the incubation concentration,[10−12] there has been no report

Received: June 16, 2017

DOI: 10.1021/jacs.7b06273
J. Am. Chem. Soc. XXXX, XXX, XXX−XXX

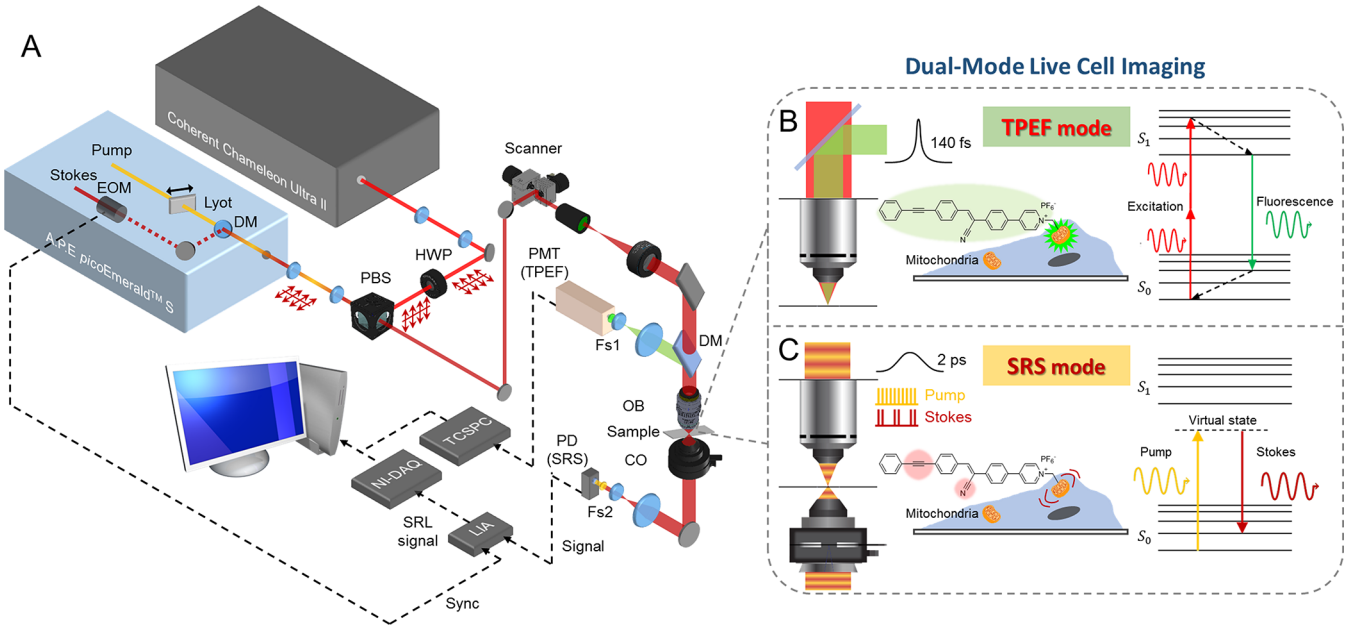

Figure 1. Dual-mode live cell imaging using FL−SRS. (A) Schematic diagram of the FL−SRS setup. Images at multiple Raman shifts were automatically acquired by tuning the pump beam wavelength to excite different Raman signals. Abbreviations: EOM (electro-optical modulator), DM (dichroic mirror), HWP (half-wave plate), PBS (polarizing beam splitter), Fs (filter set), PMT (photomultiplier tube), PD (photodiode), TPEF (two-photon excited fluorescence), SRL (simulated Raman loss), TCSPC (time-correlated single photon counting), LIA (lock-in amplifier), OB (objective), CO (condenser). (B) In TPEF mode, the 140 fs laser beam with high peak power was used to excite the fluorescence of AIE-SRS-Mito efficiently. (C) In SRS mode, the 2 ps laser beams with high spectral resolution severed as pump and Stokes beams to probe the SRS signals from the alkyne and cyano groups of AIE-SRS-Mito.

precisely evaluating the AIE dye distribution inside a live cell noninvasively because the fluorescence yield from the AIE probe is particularly sensitive to the cellular microenvironment.

Raman microscopy is emerging as a powerful noninvasive method to assess and image cellular chemical components. Complementary to fluorescence microscopy, it has become more and more common in biological research as it possesses a label-free capability and provides rich chemical information from the molecular vibrations.[13] Competing with spontaneous Raman scattering and coherent anti-Stokes Raman scattering (CARS), stimulated Raman scattering (SRS) microscopy has emerged as a superior technique for fast imaging of live cells due to its merits of (i) a greatly elevated Raman signal with a ∼1000 times faster speed than that of spontaneous Raman microscopy, (ii) excellent stability and reproducibility, (iii) elimination of nonresonant background, (iv) a linear concentration dependence, and (v) perfect spectral resemblance to spontaneous Raman spectra.[14] During the past few years, SRS has found great success in the cell-silent vibrational region (1800−2800 cm^{-1}) because it can efficiently eliminate C−H interference, which is ubiquitous in nearly all biomolecules, including proteins, nucleosides, triglycerides, and cholesterol from 2800 to 3100 cm^{-1}.[15,16] Small biorthogonal imaging tags such as stable-isotope labeling (C−D, ^{13}C) and triple bonds (alkyne C≡C, cyano C≡N) and their combined technology have opened a new window for specifically tracking newly uptaken small biomolecules in DNA, proteins, lipids, sugars, and drugs.[16−26] More recently, SRS imaging of alkyne-tagged cholesterol has been reported with a detection limit down to the level of 31 μM, making it promising to visualize the intracellular distribution of the target molecules in live cells with high spatiotemporal resolution.[27] In this work, we combine fluorescence microscopy with SRS microscopy to make new features in cell imaging. Considering the unique advantages of the two different modalities, it is beneficial to develop dual-mode probes and image live cells from two perspectives.[28] We anticipate this cross-microscopy system will enable us to study a wide range of samples and to detect the biodistribution more accurately, together with the capability of rapid *in vivo* imaging.

Among all the cellular organelles, mitochondria play a critical role in cell metabolism, including energy supply, signaling regulation, and apoptosis.[29−33] They often serve as the targets of toxicants, drugs, and other functionalized molecules to induce various biological effects.[32,34−38] Therefore, imaging the mitochondrial dynamics and studying their related biological processes are becoming more and more important for physiological and pathological studies.[33,39−42] So far, many AIE fluorescent mitochondrion-targeting probes have been reported, or even commercialized, and many fluorescent molecules have been reported to be mitochondrion-targeting with therapeutic effects (photodynamic therapy, chemical therapy, etc.), especially against cancers.[12,38,42−45] However, little work on *in vivo* quantitative measurement of dye distribution in mitochondria was conducted. Previously, mitochondria were identified by the spontaneous Raman signal from cytochrome *c* in the vibrational fingerprint region.[17,18,46] Another report developed an alkyne-tagged Raman marker for mitochondria imaging, named MitoBADY, to improve the image contrast.[47] The drawback is that both of these studies utilized spontaneous Raman with high interference and an extremely long integration time, which do not allow dynamic imaging in live cells. Moreover, cytochrome *c* and MitoBADY are not suitable for multimodal nonlinear optical (NLO) imaging due to their low absorption cross-section and UV excitation/emission.

DOI: 10.1021/jacs.7b06273
J. Am. Chem. Soc. XXXX, XXX, XXX−XXX

To prove the concept of dual-mode imaging, herein, by rational design and simple chemical synthesis, we demonstrate a diphenylacetylene-containing AIE probe, named AIE-SRS-Mito, for imaging mitochondria in live cells via both fluorescence (FL) and SRS imaging modalities. Taking advantage of the linear concentration dependence of SRS and inertness of the alkyne Raman signal to environmental change, we quantify the intracellular distribution of AIE-SRS-Mito via the SRS signal intensity. Furthermore, colocalization of the FL and SRS images reveals the positive correlation between FL and SRS signals, confirming the nonquenching effect of such AIE molecules with an increase of concentration observed in cell imaging. In this study, we demonstrate the utility of our dual-mode microscopy to reveal the local concentration of AIE molecules at the subcellular level for the first time. In a wider scope, our FL−SRS imaging strategy can be applied to other similar dual-mode FL−SRS probes to illustrate their intracellular location and evolution process. This work will potentially promote the development of dual-mode probes with varied intracellular targeting and the utilization of the corresponding FL−SRS microscopy, thus benefiting subcellular organelle studies under physiological and pathological conditions.

EXPERIMENTAL SECTION

Materials and Characterization. Minimum essential medium (MEM), fetal bovine serum (FBS), penicillin, streptomycin, and Mitotracker Red FM were purchased from Invitrogen. 3-(4,5-Dimethylthiazol-2-yl)-2,5-diphenyltetrazolium bromide (MTT), other chemicals, and solvents were all purchased from Sigma-Aldrich and used as received without further purification. Milli-Q water was supplied by the Milli-Q Plus System (Millipore Corp., Bedford, MA). Milli-Q water (18.2 MΩ) was used to prepare the buffer solutions. 1× PBS contains NaCl (137 mM), KCl (2.7 mM), Na_2HPO_4 (10 mM), and KH_2PO_4 (1.8 mM). ^1H and ^{13}C NMR spectra were measured on a Bruker ARX 400 NMR spectrometer using DMSO-d_6 and $CDCl_3$ as solvents and tetramethylsilane (TMS) as an internal reference. High-resolution mass spectra were recorded on a Finnigan MAT TSQ 7000 mass spectrometer system operating in a MALDI-TOF mode. The spontaneous Raman spectra were measured using a micro-Raman/photoluminescence spectroscopy system (InVita, Renishaw RM 3000) at room temperature. A 632.8 nm, 10 mW He−Ne laser was focused on the samples with a 50× objective (0.55 numerical aperture (NA)), and the integration time was ∼30 s for a single Raman spectral curve ranging from 400 to 4000 cm^{-1} or from 2000 to 2400 cm^{-1}. Photoluminescence (PL) spectra were recorded on a PerkinElmer spectrofluorometer (LS 55). Theoretical calculations were performed with density functional theory at the B3LYP/6-31G** level for geometry optimizations and the HOMO and LUMO in the Schrödinger program.

FL−SRS Microscopy. The FL−SRS imaging method and experimental setup (Figure 1) are described in detail in the Supporting Information. Briefly, a pump-laser-integrated one-box optical parametric oscillator (OPO) system (*pico*Emerald S, APE, Berlin, Germany) was used as the light source for SRS imaging. It consists of a Stokes beam (1031 nm, 2.1 ps, 80 MHz repetition rate) modulated at 20 MHz and a pump beam tunable from 780 to 960 nm (1.9 ps, 80 MHz repetition rate). In the two-photon excited fluorescence (TPEF) imaging modality, a femtosecond Ti:sapphire laser with a 140 fs pulse duration (Chameleon Ultra II, Coherent, Santa Clara, CA) was tuned at 780 nm and used as the two-photon excitation beam. The femtosecond laser was rotated from p-polarization to s-polarization by a half-wave plate (SAHWP05M-1700, Thorlabs) and combined with picosecond lasers through a polarizing beam splitter. The combined beams were sent into a homemade upright laser-scanning microscope. A water immersion objective (UAPO40XW3/340, 1.15 NA, Olympus, Japan) with high near-IR transmission was used to focus the excitation beams into the examined samples and to collect the backscattered TPEF signals. A dichroic mirror (FF665-Di02, Semrock) was placed above the objective to reflect the TPEF signals to a hybrid photomultiplier tube (PMT) detector and a time-correlated single photon counting (TCSPC) module (HPM-100-40 and SPC-150, Becker & Hickl GmbH) for photon count recording. The forward-going pump and Stokes beams, after passing through the sample, were collected in transmission with a high-NA oil immersion condenser (UAAC, Achromat/aplanat condenser, 1.4 NA, Olympus, Japan) following Köhler illumination. A high optical density (OD) short-pass filter (86108 short pass at 975 nm OD4, Edmund Optics) and band-pass filter (FF01-850/310, SRS imaging emission filter, Semrock) were used to block the Stokes beam completely and transmit the pump beam only in front of a large-area (10 × 10 mm) Si photodiode (S3590-08; Hamamatsu). The output current of the photodiode was then fed into a radio frequency lock-in amplifier (APE, Berlin, Germany) with a 20 μs time constant. The amplitude output from the lock-in amplifier (LIA) was fed back into an acquisition card (PCIe-6363, National Instruments, Austin, TX) to reconstruct the SRS image.

For the hyperspectral SRS (hsSRS) sweeping mode in solution, the pump beam wavelength of the *pico*Emerald S was tuned sequentially by a home-built C# program through serial communication. For the alkyne SRS imaging, we adjusted the Lyot filter inside the laser (while fixing the OPO crystal temperature), and a pair of "alkyne-on" and "alkyne-off" images could be acquired within a 3 s tuning time to avoid movement of the cells.[48] The final alkyne SRS image was obtained by subtracting the off-resonant signals from on-resonant signals after the imaging session.[49] Each frame was acquired within 8 s for both TPEF and SRS with a 25.6 μs pixel dwelling time, generating an image of 512 × 512 pixels.

Laser powers after the 40× IR objective used for cell imaging are as follows: 30 mW for the pump beam, 100 mW for the modulated Stokes beam of 2223, 2160, 2125, 2065, and 752 cm^{-1} channels, and 50 mW for the Stokes beam of 2950 and 2845 cm^{-1} channels. For TPEF imaging, the 780 nm laser at the sample was controlled as low as 4 mW to exclude any possible photodamage and photobleaching.

Cell Culture. HeLa cells were cultured in MEM containing 10% (v/v) FBS and antibiotics (100 units/mL penicillin and 100 g/mL streptomycin) in a humidity incubator with an atmosphere of 5% CO_2 at 37 °C and subcultured every 2−3 days.

Cell Imaging. HeLa cells were grown overnight on a 35 mm Petri dish with a coverslip. The coverslip was mounted onto an iron slide with an observation window. The staining solution was prepared by adding a dye stock solution (10 mM in DMSO) to 2 mL of the cell medium. Before imaging, the cells were stained with 2 mL of dye solution for a certain length of time and then imaged under an FL microscope (BX41 upright microscope) using different combinations of excitation and emission filters for each dye. The parameters of the optical mirrors for each channel are as follows: CH2 WIB, EX 460−490, EM 515, DM 505; CH3 WG, EX 510−550, EM 590, DM 570; CH5 Aqua, EX 400−440, EM 465, DM 455; CH6, bright field.

Cell Viability Evaluated by MTT Assay. Cells were seeded in 96-well plates at a density of 10000 cells per well. After 24 h of incubation, the medium in each well was replaced by 100 μL of fresh medium containing different concentrations of AIE-SRS-Mito. After 24 h of treatment, into each well was added 10 μL of MTT solution (5 mg/mL in PBS). After 4 h of incubation, the MTT-containing solution was gently removed and replaced with 100 μL of DMSO. After agitation, the absorption of each well at 490 nm was recorded via a plate reader (PerkinElmer Victor3). Each of the experiments was performed with six wells parallel. The background of the blank was subtracted, and the cell viability of the control group was set to unity.

RESULTS AND DISCUSSION

Design and Synthesis of AIE-SRS-Mito. α-Cyanostilbene has been reported to be a good building block for generating AIE fluorophores (AIEgens) with different emissions by

DOI: 10.1021/jacs.7b06273
J. Am. Chem. Soc. XXXX, XXX, XXX−XXX

attaching various donor groups to its molecular structure.[50,51] Recently, our group reported an AIE fluorophore, named ASCP (Scheme 1), that consists of α-cyanostilbene as the AIE

Scheme 1. Design Strategy and Synthetic Route of AIE-SRS-Mito (1)[a]

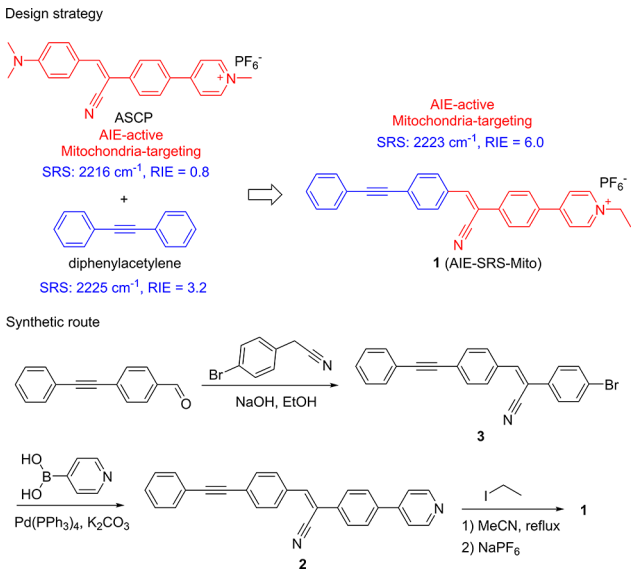

[a]The SRS peak position and relative Raman intensity versus EdU (RIE) are noted.

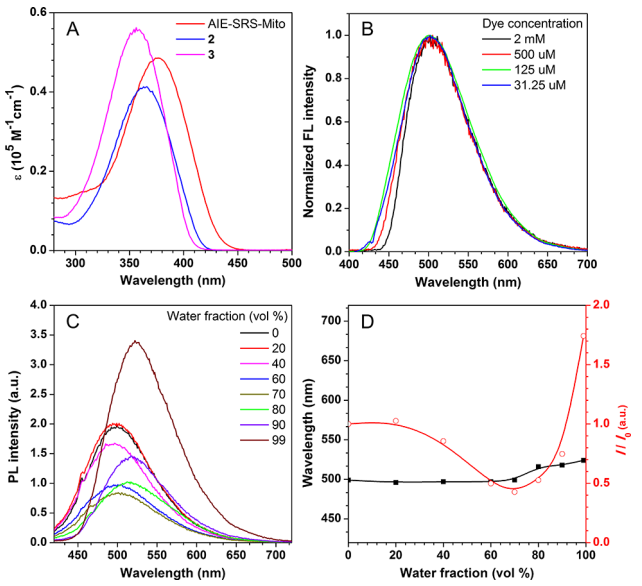

Figure 2. Photophysical properties of AIE-SRS-Mito. (A) UV–vis absorption spectra of AIE-SRS-Mito and its precursors in DMSO. (B) Fluorescence (FL) spectra of AIE-SRS-Mito in DMSO with different concentrations. Excitation wavelength 380 nm. (C) FL spectra of AIE-SRS-Mito in DMSO–water mixtures with various water fractions. (D) Peak wavelength and peak intensity of AIE-SRS-Mito in DMSO–water mixtures versus the water fraction. Dye concentration 10 μM. Excitation wavelength 400 nm.

skeleton and pyridinium salt as the targeting group for mitochondria.[52] Although it has a biorthogonal Raman peak at 2216 cm^{-1} for the C≡N group (Figure S1, Supporting Information), the intensity of RIE (relative Raman intensity versus 5-ethynyl-2′-deoxyuridine (EdU)) is 0.8 in the cell-silent vibrational region at 2216 cm^{-1}, much lower than that of AIE-SRS-Mito (RIE = 6.0). Diphenylacetylene is reported to have a biorthogonal Raman signal peak at 2225 cm^{-1} with a moderate Raman cross-section,[18] and this molecule is also easy to incorporate into the π-conjugated molecule synthetically to improve the SRS intensity. Therefore, we expected to have a mitochondrion-targeting probe with an AIE feature and a biorthogonal Raman signal by creating a hybrid of ASCP and diphenylacetylene. Simply following the synthetic procedures of ASCP by replacing the 4-(dimethylamino)benzaldehyde with commercially available 4-(phenylethynyl)benzaldehyde, AIE-SRS-Mito was obtained in three sequential steps of Knoevenagel condensation, Suzuki coupling, and alkylation (Scheme 1). Detailed preparation procedures can be found in the Supporting Information. The structure of AIE-SRS-Mito and its synthetic precursors (compounds **2** and **3**) were confirmed by ^{1}H NMR, ^{13}C NMR, high-resolution mass, and spontaneous Raman spectroscopies with satisfactory results (Supporting Information, Figures S2–S15).

Photophysical Properties. After structure confirmation, the photophysical properties of AIE-SRS-Mito were investigated. As shown in Figure 2A, AIE-SRS-Mito exhibited a redder absorption band at around 380 nm than its synthetic precursors. The red shift can be attributed to the extension of π-conjugation and the enhanced electron-accepting property of the pyridinium salts. On the other hand, the fluorescence band of AIE-SRS-Mito was located at around 500 nm, giving a large Stokes shift of 120 nm (Figure 2B), due to the twisted intramolecular charge transfer (TICT) effect. Because of such a large Stokes shift, only a slight inner-filter effect was observed when the solution concentration was increased from 31.25 μM to 2 mM, as suggested by a little change in the peak wavelength and a slight decrease in emission intensity at wavelengths below 480 nm. Compared to ASCP (Table S1, Supporting Information),[52] both the absorption and emission peaks of AIE-SRS-Mito are blue-shifted due to the weaker electron-donating ability of the phenylacetylene group than the dimethylamine group. However, the quantum yields of AIE-SRS-Mito (1.1% in DMSO and 13% in the solid state) are significantly higher than those of ASCP (0.2% in DMSO and 0.7% in the solid state). The higher quantum yield in the solid state exhibits the typical AIE characteristic. Moreover, both of the probes were found to be two-photon-excitable by a 140 fs laser at 800 nm, and their two-photon absorption cross sections were determined to be 14.2 and 61.9 GM for AIE-SRS-Mito and ASCP, respectively (Table S1). Such values are moderate compared to those of previously reported two-photon fluorophores and probes.[53,54]

Next, to further illustrate the AIE feature of AIE-SRS-Mito, it was studied in DMSO–water mixtures with different water fractions. As shown in Figure 2C,D, the emission intensity decreased with an increase in the water fraction from 0 to 70 vol % due to the enhancement of the TICT effect by the increase in the polarity of the surrounding environment upon water addition. Due to the poor solubility of AIE-SRS-Mito in water, further increasing the water fraction led to the formation of molecular aggregates, accompanied by an increase in the fluorescence intensity. This demonstrates a typical AIE phenomenon. Upon aggregation, the free intramolecular rotations of the excited molecules are restricted. This blocks the nonradiative relaxation pathway and favors the radiative decay.[9] The AIE feature and TICT effect of the dye molecule

DOI: 10.1021/jacs.7b06273
J. Am. Chem. Soc. XXXX, XXX, XXX–XXX

were further verified by theoretical calculations (Figure S16, Supporting Information). The results revealed that AIE-SRS-Mito took a twisted conformation like other AIEgens. A substantial shift of the electron cloud from HOMO to LUMO was observed, suggesting a TICT characteristic.

Mitochondrion-Selective Staining. Cell permeability is an important factor to evaluate the performance of a probe. We found that AIE-SRS-Mito exhibited a good cell permeability, while its synthetic precursors were hardly able to stain the cells (Figure S17, Supporting Information). We also conducted a colocalization experiment to verify the mitochondrial specificity of AIE-SRS-Mito. As shown in Figure 3A–D, AIE-SRS-Mito

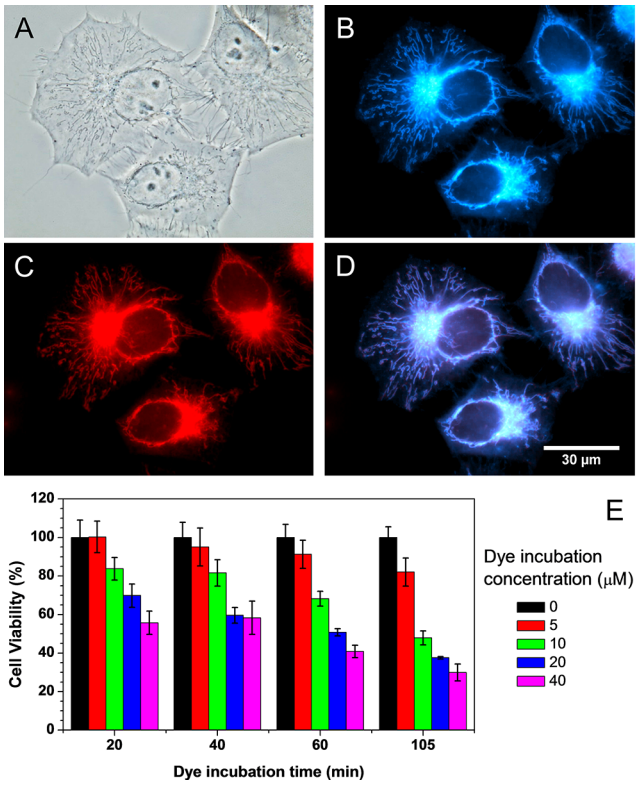

Figure 3. Mitochondrial specificity and MTT assay of AIE-SRS-Mito. (A) Bright-field and fluorescent images of HeLa cells costained with (B) AIE-SRS-Mito (5 μM) and (C) Mitotracker Red FM (MTR, 100 nM) in culture medium for 20 min. (D) Merged image of (B) and (C). Excitation wavelength 330–385 nm for AIE-SRS-Mito and 540–580 nm for MTR. (E) Cell viability tested by MTT assay. HeLa cells were incubated with different concentrations of AIE-SRS-Mito for 20, 40, 60, or 105 min for mitochondrial staining. The cells were cultured in fresh medium for 24 h after staining.

stained the linear reticulum-like structures in cells with high contrast, and its fluorescence was perfectly overlapped with the fluorescence of a commercial mitochondrial probe, Mitotracker Red FM (MTR), revealing the good mitochondrial selectivity of AIE-SRS-Mito. To evaluate whether the probe can serve as a mitochondrial probe, biocompatibility is of concern. Thus, we evaluated the cell cytotoxicity of AIE-SRS-Mito by MTT assay. In Figure 3E, the results showed that the toxicity of AIE-SRS-Mito indeed increased with increasing dye incubation concentration and dye incubation time. Longer incubation time and higher dye incubation concentration would cause overload of the dye molecules in cells and ultimately lead to lower viability over 24 h. This may be attributed to the fact that the presence of a high concentration of cationic dyes in the mitochondrial matrix would cause depolarization and increase the osmotic stress of the organelles.[38,43] In our following SRS imaging experiments, the staining condition was 5 μM AIE-SRS-Mito for 60 min of incubation. On the basis of the MTT results in Figure 3E, this condition does not cause any significant cytotoxicity (ca. 90% cell viability over 24 h). Good-quality FL/SRS images could be obtained under this staining condition as shown in the following section. Our imaging was also conducted within 1 h after staining according to the protocol,[55] and no obvious decrease in signal was observed. Therefore, our probe is capable of mitochondrial imaging via FL and SRS with good biocompatibility and low toxicity.

To study the mitochondrial morphologies under low and high dye incubation concentrations, experiments were carried out by incubating the HeLa cells with 5 and 20 μM AIE-SRS-Mito for 30, 60, and 105 min. Meanwhile, all the cells were costained with MTR to indicate the location of mitochondria. The results showed that at a lower concentration of 5 μM (Figure S18, Supporting Information) AIE-SRS-Mito exhibited a high specificity to mitochondria with a low background. The tubular reticulum-like mitochondrial morphologies indicated that the cells were healthy. However, at a higher incubation concentration of 20 μM (Figure S19, Supporting Information), the mitochondria of the cells still showed tubular reticulum-like structures for the incubation time of 30 min, and they became segmental granular structures for longer incubation times of 60 and 105 min, suggesting the unhealthy cell states caused by the overload of dyes, which are consistent with the MTT results. Also, other cellular structures were stained when the incubation time was 105 min (Figure S19). This result suggested that the higher dosage of AIE-SRS-Mito would cause the loss of the specificity to mitochondria.

SRS and TPEF Properties. Using our homemade FL–SRS microscope, we investigated the Raman scattering signal of AIE-SRS-Mito. Resembling its own spontaneous Raman spectrum (Figure S15), AIE-SRS-Mito showed a Raman peak at 2223 cm^{-1} in the cell-silent region with a peak intensity of RIE = 6.0 (Figure 4A), which is a factor of 8 higher than that of ASCP. Such a high RIE value should be attributed to the synergetic effect of the signals of diphenylacetylene (C≡C, 2225 cm^{-1}, RIE = 3.2) and cyanostilbene (C≡N, 2206 cm^{-1}, RIE = 1.3) (Figure 4A and Figure S20, Supporting Information). Furthermore, the SRS spectra of AIE-SRS-Mito were collected at different dye concentrations in DMSO, and the results showed that no obvious Raman peak shift was found (Figure S21, Supporting Information), indicating the inertness of the Raman signal to the concentration change. To suppress the non-Raman backgrounds, including cross-phase modulation, transient absorption, and thermal lensing effects, the SRS intensities I_{ON} at 2223 cm^{-1} (on-resonance) and I_{OFF} at 2160 cm^{-1} (off-resonance or reference) were used to calculate the genuine SRS signal intensity, $I_{SRS} = I_{ON} - I_{OFF}$.[49] In this way, a linear relationship between the SRS intensity I_{SRS} and the dye concentration c of AIE-SRS-Mito was obtained as $I_{SRS} = 0.1567c$ ($R^2 = 0.99944$, Figures 4B and S21). Also, its analytical detection limit and quantification limit were calculated to be 8.5 μM and 28.4 μM (Table S2, Supporting Information), respectively. Due to the inert response of the SRS signal to the environmental change and suppression of non-Raman backgrounds, the linear plot of $I_{SRS} = 0.1567c$ can act further as a calibration for the intracellular dye concentration by keeping the same signal excitation and collection conditions. In

DOI: 10.1021/jacs.7b06273
J. Am. Chem. Soc. XXXX, XXX, XXX–XXX

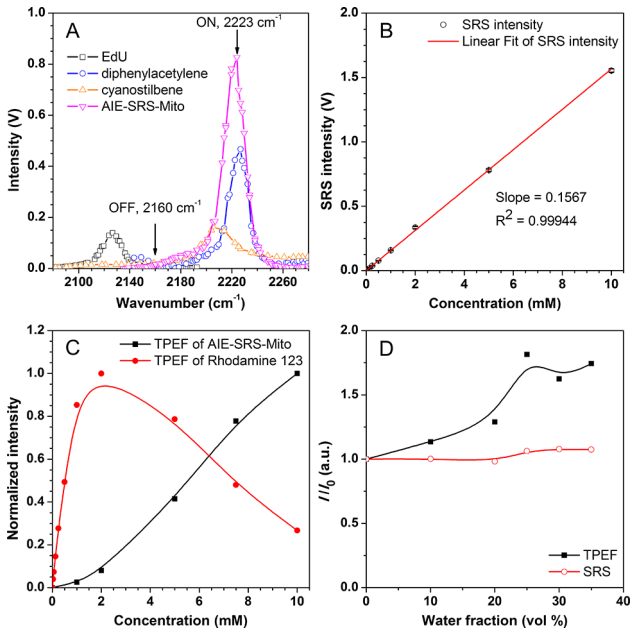

Figure 4. SRS and TPEF properties of AIE-SRS-Mito. (A) hsSRS sweeping of EdU (5 mM in PBS) or AIE-SRS-Mito (5 mM in DMSO) in cell-silent region. (B) Change of the SRS intensity I_{SRS} of AIE-SRS-Mito with different concentrations (the background from DMSO was subtracted, $I_{SRS} = I_{ON} - I_{OFF}$). (C) Change of the TPEF intensity of Rhodamine 123 and AIE-SRS-Mito with different concentrations (0–10 mM). (D) TPEF and SRS of AIE-SRS-Mito (1 mM) in DMSO–water mixtures with different water fractions.

comparison with a previous study,[21] the analytical detection limit and quantification limit of EdU were also calculated to be 169.7 and 565.5 μM (Figures S22 and S23 and Table S3, Supporting Information).

To gain further understanding of the inertness of the SRS signal, two factors, namely, concentration and polarity, were examined. TPEF was used for this demonstration due to the simultaneous dual-mode acquisition feasibility and high near-infrared (NIR) beam throughput rate of our FL–SRS system. As a newly synthesized compound, the two-photon excitation maximum was found to be 780 nm for AIE-SRS-Mito (Figure S24, Supporting Information) and was used for the following experiments. As shown in Figure 4C, nonlinearities of fluorescence intensity versus concentration were observed for both AIE-SRS-Mito and Rhodamine 123 in the range of 0–10 mM. Here, Rhodamine 123, a structural derivative of fluorescein, is used as a representative of ACQ fluorophores, while AIE-SRS-Mito is an AIE probe. The occurrence of fluorescence quenching of Rhodamine 123 was found to be lower than 1 mM, which may have been caused by the self-absorption, severe collisions of excited molecules, formation of nonfluorescent excimers, etc.[56] Meanwhile, AIE-SRS-Mito was found to be more resistant to fluorescence quenching at high concentration. In terms of the polarity effect, the TPEF and SRS signals were studied simultaneously in DMSO–water mixtures at a concentration of 1 mM (Figure 4D). With an increase in the water fraction from 0 to 40 vol % (further increasing the water fraction would lead to severe aggregation), the SRS intensity exerted little change, while the TPEF intensity increased almost by 70%. Lowering the concentration to 10 μM also showed a similar trend, and the TPEF intensity increased almost by 40% (Figure S25, Supporting Information). However, the TPEF intensity of Rhodamine 123 increased by 250% (Figure S26, Supporting Information). The above results demonstrate well the high sensitivity of the fluorescence intensity and inertness of the SRS intensity to changes in concentration and the surrounding environment, confirming that SRS is superior to fluorescence for concentration calibration in a heterogeneous intracellular environment.

SRS Imaging in Live Cells. Using our homemade SRS system, images with a 100 × 100 μm field of view (FOV) and 512 × 512 pixels were obtained at a speed of 8 s/frame. An even faster speed of 1 s/frame can be achieved under the condition of sufficient signal intensity, demonstrating the fast imaging capability of our SRS system. To validate our homemade SRS imaging system, SRS imaging was conducted with live HeLa cells. Figure 5 shows the distributions of

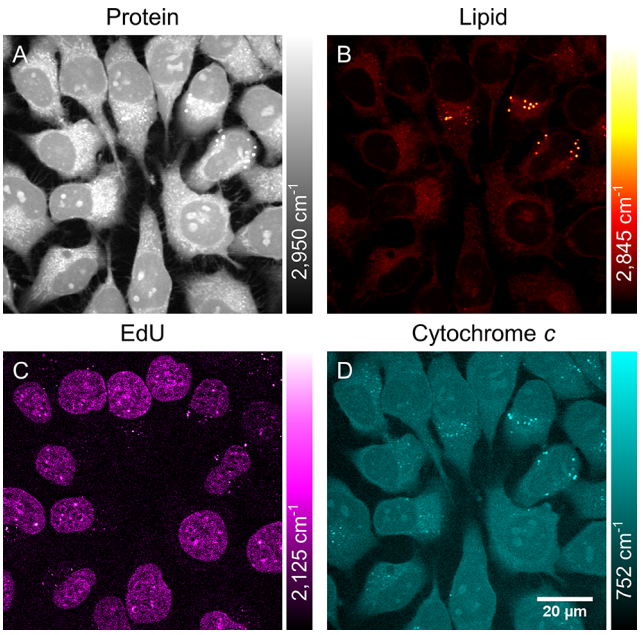

Figure 5. SRS images of different chemical components in live HeLa cells. (A) Protein at 2950 cm^{-1}. (B) Lipid at 2845 cm^{-1}. (C) Nuclei labeled by EdU at 2125 cm^{-1}. (D) Cytochrome *c* at 752 cm^{-1}. HeLa cells were pretreated with 100 μM EdU for 22 h.

proteins, lipids, DNA, and cytochrome *c* in the HeLa cells at 2950, 2845, 2125, and 752 cm^{-1}, respectively, demonstrating the vast applications of the SRS imaging in live cells. In Figure 5C, the DNA of HeLa cells was prelabeled with EdU by incubation with 100 μM EdU in culture medium for 22 h to ensure sufficient cell uptake.[17,21,22] EdU is an analogue of thymidine and can be incorporated into newly synthesized DNA during the DNA duplication (S-phase), whereas cells without DNA duplication will not incorporate EdU into their nucleus region. In SRS imaging of EdU, to suppress the non-Raman backgrounds, the "alkyne-off" image was subtracted from the "alkyne-on" image to reconstruct the final image (as shown in Figure S27, Supporting Information). This method was termed intensity-modulated stimulated Raman loss imaging (IM-SRL).[49] The SRS intensity in each pixel of the resultant image reflected the local concentration due to the proportional correlation of SRS intensity ($I_{SRS} = I_{ON} - I_{OFF}$) and the concentration *c*. Therefore, the determination of the intracellular local concentration of EdU was achieved. As indicated by the SRS images of EdU (Figures 5C and 6B,D), EdU was

DOI: 10.1021/jacs.7b06273
J. Am. Chem. Soc. XXXX, XXX, XXX–XXX

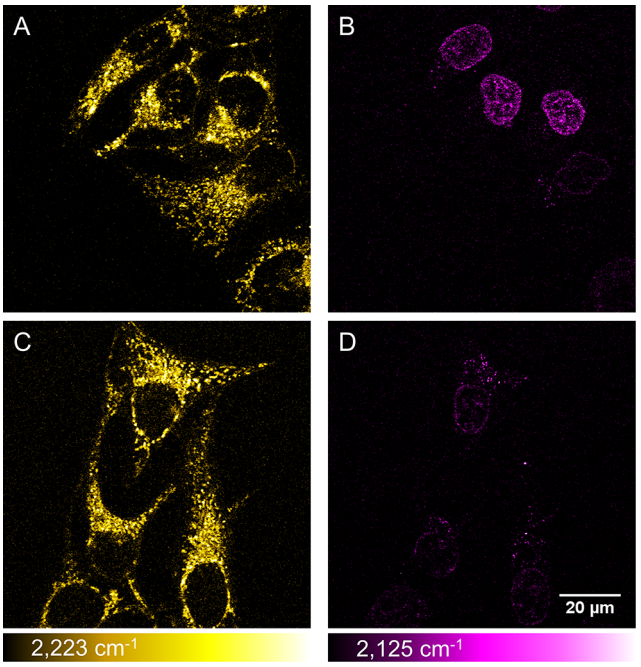

Figure 6. Dual-color chemical imaging using AIE-SRS-Mito and EdU. SRS images of (A, C) AIE-SRS-Mito and (B, D) EdU in live HeLa cells. HeLa cells were incubated with 100 μM EdU for 22 h and 5 μM AIE-SRS-Mito for 1 h.

incorporated and enriched in the nucleus regions of a part of the cells, suggesting these cells have undergone DNA synthesis over a 22 h EdU incubation time. Previously, EdU was detected by click reaction with fluorescent probes, and the detection can only be carried out in fixed cells.[11] Using SRS imaging, EdU can be detected in the live cells quantitatively and noninvasively.

Due to the high Raman signal (RIE = 6.0) at 2223 cm^{-1} and mitochondrion-targeting capability of AIE-SRS-Mito, we expected that AIE-SRS-Mito could serve as a mitochondrial probe for Raman microscopy. In previous reports, cytochrome *c* (Raman signal at 752 cm^{-1}), an endogenous protein abundant in the mitochondrial membrane, was used for visualization of the mitochondria.[17,18,46] However, only an unclear image of low contrast was obtained (Figure 5D). The mitochondrial features did not appear in the SRS image as in the previously reported spontaneous Raman image.[17,18,46] We also could not identify the signature Raman peak of cytochrome *c* at 750 cm^{-1} in the SRS spectrum of mitochondria (Figure S28). This further demonstrates that cytochrome *c* is not an applicable mitochondrial marker in SRS microscopy. In contrast, after incubation of HeLa cells with 5 μM AIE-SRS-Mito for 60 min, the SRS images obtained by the IM-SRL method show high-contrast fine structures of mitochondria (Figure 6A,C and Figure S27, Supporting Information). Meanwhile, compared to images of the cell nuclei or EdU (Figure 6B,D), the total discrepancy of two signals demonstrates the compatibility of using AIE-SRS-Mito together with EdU for dual-color imaging. Such a multicolor-labeling method is routinely practiced in fluorescence microscopy for visualization, localization, and study of interactions of targets of interest.[57−59] Compared to the uneven distribution of EdU between cells, AIE-SRS-Mito exhibits a rather even distribution and similar signals in the cytoplasm. Also, due to its good cell permeability, cell staining of AIE-SRS-Mito took a much shorter time (60 min) than that of EdU (22 h). In all, AIE-SRS-Mito can serve as a mitochondrial probe for SRS imaging with quick staining efficiency and good imaging contrast.

FL−SRS Imaging. We have determined AIE-SRS-Mito to be capable of dual-mode mitochondrial imaging via FL and SRS separately. Next, we performed the dual-mode imaging of the AIE-SRS-Mito in live cells to study the intracellular concentration of the AIE probe by using the quantitative SRS intensity. First, as shown in Figure 7, images of the HeLa cells

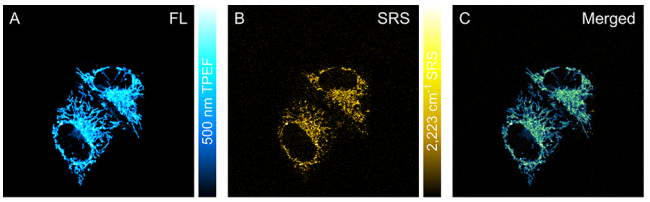

Figure 7. Colocalization of (A) TPEF and (B) SRS of HeLa cells stained with 20 μM AIE-SRS-Mito for 30 min at a low toxicity level. (C) Merged image of (A) and (B).

stained by AIE-SRS-Mito were collected by TPEF and SRS signals, respectively, and the merged image indicated a perfect colocalization of the intracellular distribution of the fluorescence and SRS signals, confirming the dual modality of the probe. Statistical analysis showed a positive correlation of the TPEF intensity and the SRS signal of AIE-SRS-Mito in cells (interpreted via the dye concentration, Figure 8A−C). The fluorescence intensity is generally not linearly correlated with the local probe concentration because the fluorescence is highly sensitive to environmental changes. The result is consistent with the fact that the biochemical environment in the cell is complex and heterogeneous. Due to the inertness of the SRS

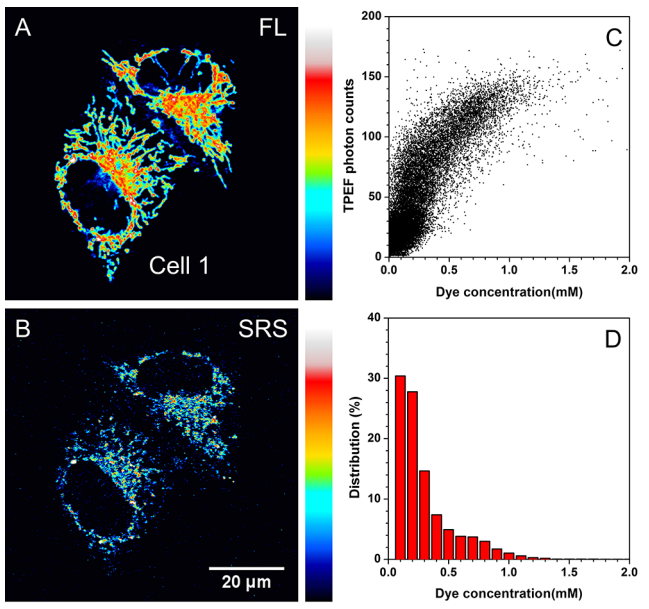

Figure 8. Statistical analysis of the fluorescence and SRS intensity of HeLa cells stained with 20 μM AIE-SRS-Mito for 30 min. (A) TPEF image. The FL intensity was coded with a royal color bar. (B) SRS image. The SRS intensity was coded with a royal color bar. (C) Correlation of the FL intensity and SRS intensity of cell 1. (D) Histogram of the dye concentration of cell 1. The SRS intensity I_{SRS} was interpreted via the dye concentration *c* by the equation I_{SRS} = 0.1567*c*.

DOI: 10.1021/jacs.7b06273
J. Am. Chem. Soc. XXXX, XXX, XXX−XXX

signal and the linear relationship (I_{SRS} = 0.1567c), we further analyzed the dye distribution inside a single cell. As shown in Figure 8D, the local concentration within a cell was found to be up to 1.5 mM, which is 75-fold higher than the incubation concentration (20 μM).

To show the potential application of the combined FL−SRS microscopy in cellular biodistribution and pharmacokinetic studies, we used AIE-SRS-Mito as a drug model of lipophilic cationic compounds to study the dosage-induced cell toxicity. The FL and SRS images from the cells treated by AIE-SRS-Mito at 20 μM with incubation times of 30, 60, and 105 min are shown in Figure 9. The FL image of cells with a 105 min

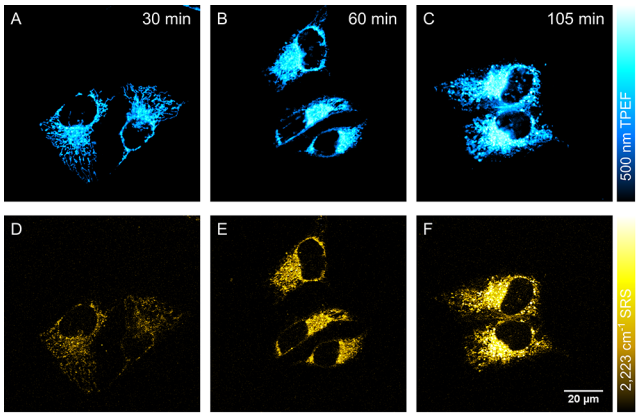

Figure 9. (A−C) Fluorescence images and (D−F) SRS images of HeLa cells stained with 20 μM AIE-SRS-Mito for (A, D) 30 min, (B, E) 60 min, and (C, F) 105 min.

incubation time showed that the reticulum-like morphology of the mitochondria shrank into granules, indicating an unhealthy cell state (Figure 9C), which is inconsistent with the MTT results in Figure 3E and the previous imaging results in Figure S19. We found that both intracellular TPEF and SRS intensities increased with an increase of the dye incubation concentration or dye incubation time (Figures S29−S31, Supporting Information). The results demonstrate that, with an increase of the dye incubation concentration or dye incubation time, more dye molecules enter into the cells and they are enriched in the mitochondrial region, causing cytotoxicity. Overall, the FL and SRS images from the cells treated with a high dye concentration and a long incubation time serve as the direct evidence to confirm the dosage-induced cell toxicity. Such results may also be applicable to other small organic dyes and drugs with cationic lipophilic features.

Furthermore, the high resolution of FL−SRS imaging enables us to study the intracellular distribution concentration of AIE-SRS-Mito at subcellular dimensions. We plot the histograms of the dye concentration distribution at each pixel within a single cell for each incubation condition used above (Figures S32 and S33, Supporting Information). At an incubation concentration of 20 μM and times of 30, 60, and 105 min, over 1% of the cell region has local dye concentrations of >1.1, 1.9, and 2.0 mM, respectively. Though such a high concentration is enough to cause the emission quenching of Rhodamine 123 in cells,[60] the TPEF intensity of AIE-SRS-Mito exhibited a positive correlation with the SRS signal (dye concentration). The results suggest that the TPEF intensity of AIE-SRS-Mito could be utilized to semiqualitatively compare the intracellular concentration without suffering from the ACQ effect, which should also be applicable to other AIE molecules. Also, to the best of our knowledge, this is the first time that the intracellular concentration and distribution of AIE probes have been determined noninvasively with high spatial resolution in living biological cells.

CONCLUSION

In summary, we have rationally designed and prepared a dual-mode AIE probe, named AIE-SRS-Mito, for selective mitochondria imaging via fluorescence and SRS microscopies. With our homemade FL−-SRS microscopy system, the peak of the SRS signal of AIE-SRS-Mito was determined to be at 2223 cm^{-1}, with a peak intensity of RIE = 6.0. The detection and quantification limits of AIE-SRS-Mito were determined to be 8.5 and 28.4 μM, respectively. Due to the inertness to environmental changes and the linear relationship with the concentration of the SRS signal, the intracellular distribution of AIE-SRS-Mito was estimated to be up to 3 mM in the mitochondria matrix on the basis of an extracellular calibration curve. Our findings suggest that Rhodamine 123 would encounter fluorescence quenching at such a high concentration, but not AIE-SRS-Mito. The positive correlation between the TPEF and SRS intensities of AIE-SRS-Mito confirms the nonquenching effect of AIEgens in live-cell imaging when the incubation concentration is increased to 40 μM. Our work will promote the study of dual-mode FL−SRS probes with various targets and the utilization of combining fluorescence with SRS microscopy. This strategy will potentially provide a complementary approach to either fluorescence or SRS microscopy of subcellular resolution, which will shed light on the spatial−temporal dynamics of many organelles and drug treatments in live cells and animals across different metabolic imaging modalities.

ASSOCIATED CONTENT

Supporting Information

The Supporting Information is available free of charge on the ACS Publications website at DOI: 10.1021/jacs.7b06273.

Detailed synthesis procedures, structural characterizations, theoretical calculations, SRS spectra, and cell imaging (PDF)

AUTHOR INFORMATION

Corresponding Authors

*tangbenz@ust.hk

*eequ@ust.hk

ORCID

Xuesong Li: 0000-0002-1795-4885

Meijuan Jiang: 0000-0002-7918-7538

Ben Zhong Tang: 0000-0002-0293-964X

Author Contributions

‖X.L. and M.J. contributed equally to this work.

Notes

The authors declare the following competing financial interest(s): X.L., M.J., B.Z.T. and J.Q. are the inventors of a patent filed by Hong Kong University of Science and Technology.

ACKNOWLEDGMENTS

We appreciate K. S. Wong's help with the measurements of quantum yields and two-photon absorption cross-sections. J.Q.

DOI: 10.1021/jacs.7b06273
J. Am. Chem. Soc. XXXX, XXX, XXX−XXX

thanks the Hong Kong Research Grants Council for financial support through Grants 662513, 16103215, 16148816, T13-607/12R, T13-706/11-1, and AOE/M-09/12 and the Hong Kong University of Science & Technology (HKUST) for financial support through Grant RPC10EG33. B.Z.T. thanks the Research Grants Council of Hong Kong (Grants 16301614, 16305015, and N_HKUST604/14) and the Innovation and Technology Commission (Grants ITC-CNERC14SC01 and ITCPD/17-9) for financial support.

REFERENCES

(1) Hell, S. W. *Nat. Biotechnol.* **2003**, *21*, 1347−1355.
(2) Chalfie, M.; Kain, S. R. *Green Fluorescent Protein: Properties, Applications and Protocols*; John Wiley & Sons: Hoboken, NJ, 2005.
(3) Sauer, M.; Hofkens, J.; Enderlein, J. *Handbook of Fluorescence Spectroscopy and Imaging: From Ensemble to Single Molecules*; Wiley-VCH: Weinheim, Germany, 2010.
(4) Sample, V.; Newman, R. H.; Zhang, J. *Chem. Soc. Rev.* **2009**, *38*, 2852−2864.
(5) Sauer, M.; Heilemann, M. *Chem. Rev.* **2017**, *117*, 7478−7509.
(6) Davis, S.; Weiss, M. J.; Wong, J. R.; Lampidis, T. J.; Chen, L. B. *J. Biol. Chem.* **1985**, *260*, 13844−13850.
(7) Emaus, R. K.; Grunwald, R.; Lemasters, J. J. *Biochim. Biophys. Acta, Bioenerg.* **1986**, *850*, 436−448.
(8) Yang, Z.; Cao, J.; He, Y.; Yang, J. H.; Kim, T.; Peng, X.; Kim, J. S. *Chem. Soc. Rev.* **2014**, *43*, 4563−4601.
(9) Mei, J.; Leung, N. L. C.; Kwok, R. T. K.; Lam, J. W. Y.; Tang, B. Z. *Chem. Rev.* **2015**, *115*, 11718−11940.
(10) Wang, E.; Zhao, E.; Hong, Y.; Lam, J. W. Y.; Tang, B. Z. *J. Mater. Chem. B* **2014**, *2*, 2013−2019.
(11) Zhao, Y.; Yu, C. Y. Y.; Kwok, R. T. K.; Chen, Y.; Chen, S.; Lam, J. W. Y.; Tang, B. Z. *J. Mater. Chem. B* **2015**, *3*, 4993−4996.
(12) Gui, C.; Zhao, E.; Kwok, R. T. K.; Leung, A. C. S.; Lam, J. W. Y.; Jiang, M.; Deng, H.; Cai, Y.; Zhang, W.; Su, H.; Tang, B. Z. *Chem. Sci.* **2017**, *8*, 1822−1830.
(13) Cheng, J.-X.; Xie, X. S. *Coherent Raman Scattering Microscopy*; CRC Press: Boca Raton, FL, 2012.
(14) Freudiger, C. W.; Min, W.; Saar, B. G.; Lu, S.; Holtom, G. R.; He, C.; Tsai, J. C.; Kang, J. X.; Xie, X. S. *Science* **2008**, *322*, 1857−1861.
(15) Tipping, W. J.; Lee, M.; Serrels, A.; Brunton, V. G.; Hulme, A. N. *Chem. Soc. Rev.* **2016**, *45*, 2075−2089.
(16) Wei, L.; Hu, F.; Chen, Z.; Shen, Y.; Zhang, L.; Min, W. *Acc. Chem. Res.* **2016**, *49*, 1494−1502.
(17) Yamakoshi, H.; Dodo, K.; Okada, M.; Ando, J.; Palonpon, A.; Fujita, K.; Kawata, S.; Sodeoka, M. *J. Am. Chem. Soc.* **2011**, *133*, 6102−6105.
(18) Yamakoshi, H.; Dodo, K.; Palonpon, A.; Ando, J.; Fujita, K.; Kawata, S.; Sodeoka, M. *J. Am. Chem. Soc.* **2012**, *134*, 20681−20689.
(19) Wei, L.; Yu, Y.; Shen, Y.; Wang, M. C.; Min, W. *Proc. Natl. Acad. Sci. U. S. A.* **2013**, *110*, 11226−11231.
(20) Fu, D.; Yu, Y.; Folick, A.; Currie, E.; Farese, R. V., Jr; Tsai, T.-H.; Xie, X. S.; Wang, M. C. *J. Am. Chem. Soc.* **2014**, *136*, 8820−8828.
(21) Wei, L.; Hu, F.; Shen, Y.; Chen, Z.; Yu, Y.; Lin, C.-C.; Wang, M. C.; Min, W. *Nat. Methods* **2014**, *11*, 410−412.
(22) Hong, S.; Chen, T.; Zhu, Y.; Li, A.; Huang, Y.; Chen, X. *Angew. Chem., Int. Ed.* **2014**, *53*, 5827−5831.
(23) Shen, Y.; Xu, F.; Wei, L.; Hu, F.; Min, W. *Angew. Chem., Int. Ed.* **2014**, *53*, 5596−5599.
(24) Chen, Z.; Paley, D. W.; Wei, L.; Weisman, A. L.; Friesner, R. A.; Nuckolls, C.; Min, W. *J. Am. Chem. Soc.* **2014**, *136*, 8027−8033.
(25) Hu, F.; Chen, Z.; Zhang, L.; Shen, Y.; Wei, L.; Min, W. *Angew. Chem., Int. Ed.* **2015**, *54*, 9821−9825.
(26) Hu, F.; Lamprecht, M. R.; Wei, L.; Morrison, B.; Min, W. *Sci. Rep.* **2016**, *6*, 39660.
(27) Lee, H. J.; Zhang, W.; Zhang, D.; Yang, Y.; Liu, B.; Barker, E. L.; Buhman, K. K.; Slipchenko, L. V.; Dai, M.; Cheng, J. X. *Sci. Rep.* **2015**, *5*, 7930.
(28) Krauss, S. D.; Petersen, D.; Niedieker, D.; Fricke, I.; Freier, E.; El-Mashtoly, S. F.; Gerwert, K.; Mosig, A. *Analyst* **2015**, *140*, 2360−2368.
(29) Lin, M. T.; Beal, M. F. *Nature* **2006**, *443*, 787−795.
(30) Scherz-Shouval, R.; Elazar, Z. *Trends Cell Biol.* **2007**, *17*, 422−427.
(31) Gogvadze, V.; Orrenius, S.; Zhivotovsky, B. *Trends Cell Biol.* **2008**, *18*, 165−173.
(32) Gogvadze, V.; Orrenius, S.; Zhivotovsky, B. *Semin. Cancer Biol.* **2009**, *19*, 57−66.
(33) Sureshbabu, A.; Bhandari, V. *Front. Physiol.* **2013**, *4*, 384.
(34) Johnson, L. V.; Walsh, M. L.; Bockus, B. J.; Chen, L. B. *J. Cell Biol.* **1981**, *88*, 526−535.
(35) Chen, Y.; Qiao, L.; Yu, B.; Li, G.; Liu, C.; Ji, L.; Chao, H. *Chem. Commun.* **2013**, *49*, 11095−11097.
(36) Simcox, E. M.; Reeve, A.; Turnbull, D. *Biochem. Soc. Trans.* **2013**, *41*, 1618−1624.
(37) Zhao, E.; Deng, H.; Chen, S.; Hong, Y.; Leung, C. W. T.; Lam, J. W. Y.; Tang, B. Z. *Chem. Commun.* **2014**, *50*, 14451−14454.
(38) Zhang, C.-J.; Hu, Q.; Feng, G.; Zhang, R.; Yuan, Y.; Lu, X.; Liu, B. *Chem. Sci.* **2015**, *6*, 4580−4586.
(39) Frezza, C.; Gottlieb, E. *Semin. Cancer Biol.* **2009**, *19*, 4−11.
(40) Zhang, L.; Liu, W.; Huang, X.; Zhang, G.; Wang, X.; Wang, Z.; Zhang, D.; Jiang, X. *Analyst* **2015**, *140*, 5849−5854.
(41) Emma, F.; Montini, G.; Parikh, S. M.; Salviati, L. *Nat. Rev. Nephrol.* **2016**, *12*, 267−280.
(42) Chennoufi, R.; Bougherara, H.; Gagey-Eilstein, N.; Dumat, B.; Henry, E.; Subra, F.; Bury-Mone, S.; Mahuteau-Betzer, F.; Tauc, P.; Teulade-Fichou, M. P.; Deprez, E. *Sci. Rep.* **2016**, *6*, 21458.
(43) Hu, Q.; Gao, M.; Feng, G.; Liu, B. *Angew. Chem., Int. Ed.* **2014**, *53*, 14225−14229.
(44) Zhao, N.; Chen, S.; Hong, Y.; Tang, B. Z. *Chem. Commun.* **2015**, *51*, 13599−13602.
(45) Shin, W. S.; Lee, M.-G.; Verwilst, P.; Lee, J. H.; Chi, S.-G.; Kim, J. S. *Chem. Sci.* **2016**, *7*, 6050−6059.
(46) Okada, M.; Smith, N. I.; Palonpon, A. F.; Endo, H.; Kawata, S.; Sodeoka, M.; Fujita, K. *Proc. Natl. Acad. Sci. U. S. A.* **2012**, *109*, 28−32.
(47) Yamakoshi, H.; Palonpon, A.; Dodo, K.; Ando, J.; Kawata, S.; Fujita, K.; Sodeoka, M. *Bioorg. Med. Chem. Lett.* **2015**, *25*, 664−667.
(48) Lu, F.-K.; Basu, S.; Igras, V.; Hoang, M. P.; Ji, M.; Fu, D.; Holtom, G. R.; Neel, V. A.; Freudiger, C. W.; Fisher, D. E.; Xie, X. S. *Proc. Natl. Acad. Sci. U. S. A.* **2015**, *112*, 11624−11629.
(49) Zhang, D.; Slipchenko, M. N.; Leaird, D. E.; Weiner, A. M.; Cheng, J.-X. *Opt. Express* **2013**, *21*, 13864−13874.
(50) Huang, C.; Peng, X.; Yi, D.; Qu, J.; Niu, H. *Sens. Actuators, B* **2013**, *182*, 521−529.
(51) Jin, Y.; Xia, Y.; Wang, S.; Yan, L.; Zhou, Y.; Fan, J.; Song, B. *Soft Matter* **2015**, *11*, 798−805.
(52) Yu, C. Y. Y.; Zhang, W.; Kwok, R. T. K.; Leung, C. W. T.; Lam, J. W. Y.; Tang, B. Z. *J. Mater. Chem. B* **2016**, *4*, 2614−2619.
(53) Drobizhev, M.; Makarov, N. S.; Tillo, S. E.; Hughes, T. E.; Rebane, A. *Nat. Methods* **2011**, *8*, 393−399.
(54) Kim, H. M.; Cho, B. R. *Chem. Rev.* **2015**, *115*, 5014−5055.
(55) Mitra, K.; Lippincott-Schwartz, J. *Curr. Protoc. Cell Biol.* **2010**, 4.25.1−4.25.21.
(56) Lakowicz, J. R. *Principles of Fluorescence Spectroscopy*; Springer: New York, 2006.
(57) Boren, J.; Brindle, K. M. *Cell Death Differ.* **2012**, *19*, 1561−1570.
(58) Shi, H.; Kwok, R. T. K.; Liu, J.; Xing, B.; Tang, B. Z.; Liu, B. *J. Am. Chem. Soc.* **2012**, *134*, 17972−17981.
(59) Zhang, W.; Kwok, R. T. K.; Chen, Y.; Chen, S.; Zhao, E.; Yu, C. Y. Y.; Lam, J. W. Y.; Zheng, Q.; Tang, B. Z. *Chem. Commun.* **2015**, *51*, 9022−9025.
(60) Duchen, M. R.; Biscoe, T. J. *J. Physiol.* **1992**, *450*, 33−61.

DOI: 10.1021/jacs.7b06273
J. Am. Chem. Soc. XXXX, XXX, XXX−XXX